
Lung Deformation Estimation and Four-dimensional CT Lung Reconstruction¹

Sheng Xu, Russell H. Taylor, Gabor Fichtinger, Kevin Cleary

Rationale and Objectives. Four-dimensional (4D) computed tomography (CT) can be used in radiation treatment planning to account for respiratory motion. Current 4D CT techniques have limitations in either spatial or temporal resolution. In addition, most of these techniques rely on auxiliary surrogates to relate the time of the CT scan to the patient's respiratory phase. We propose a 4D CT method for lung applications to overcome these problems.

Materials and Methods. A set of axial scans are taken at multiple table positions to obtain a series of two-dimensional images while the patient is breathing freely. Each two-dimensional image is registered to a reference CT volume. The deformation of the image with respect to the volume is used to synchronize the image with the respiratory cycle assuming that there is no phase variation along the craniocaudal direction. The reconstructed 4D dataset is a series of deformable transformations of the reference volume.

Results. A synthetic 4D dataset showed that the registration error is less than 5% of the image deformation. A swine study showed that the algorithm can generate better image quality than the image sorting method. A respiratory-gated 4D dataset showed that the algorithm's result is consistent with the ground truth.

Conclusion. The algorithm can reconstruct good quality 4D images without external surrogates even if the CT scans are acquired under irregular respiratory motion. The algorithm may allow for reduced radiation dose to the patient with a limited loss of image quality. Although the phase variation exists along the craniocaudal direction, the 4D reconstruction is reasonably accurate.

Key Words. 4D CT; deformable image registration; lung cancer; motion compensation; respiratory motion.

© AUR, 2006

Lung cancer is the leading cause of cancer death of both men and women, resulting in more deaths than prostate cancer, breast cancer, and colon cancer combined in 2002 (1). Radiation therapy has been used to treat lung cancer by delivering high-energy x-rays to destroy cancer cells.

However, because of respiratory motion, accurate and efficient radiation delivery is difficult. Four-dimensional (4D) computed tomography (CT) is a technique that can account for respiratory motion in treatment planning, allowing for the reduction of target volume margin to achieve increased tumor dose and decreased normal tissue dose (2). Although the radiation dose to the patient from CT scanning may be an issue, particularly if multiple 4D datasets are considered; in general, the CT dose will be much less than the treatment dose delivered during radiation therapy. 4D CT may also be used to investigate the motion correlation between the internal tumor and external fiducials such as skin markers. The tumor position could then be estimated during the treatment by tracking the external fiducials. With sufficient 4D CT datasets, a

Acad Radiol 2006; 13:1082-1092

¹ From Philips Research North America, 345 Scarborough Road, Briarcliff Manor, NY, 10510 (S.X.), Engineering Research Center, Johns Hopkins University, Baltimore, MD (R.H.T., G.F.), and Imaging Science and Information Systems (ISIS) Center, Department of Radiology, Georgetown University Medical Center, Washington, DC (K.C.). Received February 1, 2006; accepted May 6, 2006. Supported by U.S. Army grants DAMD17-99-1-9022 and W81XWH-04-1-0078, NSF Engineering Research Center 9731478. **Address correspondence to:** S.X. e-mail: sheng.xu@philips.com

© AUR, 2006

doi:10.1016/j.acra.2006.05.004

respiratory model might also be constructed to parameterize the respiratory motion.

Most 4D lung reconstruction algorithms reported in the literature can be grouped into the following two approaches. The first approach requires controlling the patient's breath during image acquisition (3). The respiratory cycle is divided into several phases—usually 7–11. The respiration is controlled in each phase using respiratory gating (4–6) while a three-dimensional (3D) CT volume is taken. A related technique is to use breathing tracking strategies such as active breathing control (7–10) to monitor the patient's breath at each phase. The 4D data acquired by this method have high spatial resolution, but very poor temporal resolution. This low temporal resolution limits its usefulness in analyzing the anatomic motion.

The second approach does not try to monitor or control the patient's breath. The patient is allowed to breathe freely on the CT table (3,11). The table is moved in small increments and a set of continuous scans is taken at each table position to cover at least one complete respiratory cycle of the patient. Some external devices may be used during the scan to synchronize the CT scan time with the respiratory phase (11,12). After image acquisition, all the free scan images are sorted into a sequence of 3D volumes according to their respiratory phase and table positions. This method has high temporal resolution at each table position. The major problem with this method is that respiratory motion is not completely repeatable, so the time stamp of the free scan image may not correlate well with the regular respiratory motion. In such a case, the image quality of the 3D data reconstructed at each respiratory phase will be very poor. It is usually very difficult to stitch these 3D volumes together into a 4D dataset.

Unlike prior methods, we propose a new 4D lung reconstruction method that has good temporal resolution and high reconstruction quality. In addition, our method does not rely on any external gating or tracking devices to synchronize the time of CT scan and the respiratory phase. Therefore, problems caused by the discrepancy between the respiratory motion and the auxiliary surrogates are avoided.

METHODS

Our 4D CT lung reconstruction method is illustrated in Fig 1. First, a reference 3D CT volume is obtained under

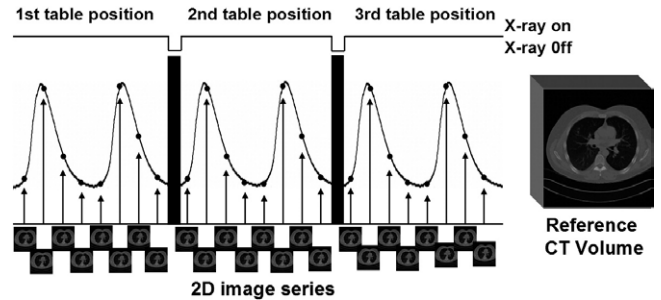


Figure 1. Four-dimensional computed tomography image acquisition [adapted from (11)].

breath hold. Next, a set of continuous CT scans is taken at every table position to obtain a series of two-dimensional (2D) images while the patient is breathing freely. The 2D image series at every table position covers at least one complete respiratory cycle. Using deformable registration, each 2D image is registered to the reference volume to estimate the displacement field of the 2D image with respect to the reference volume. The respiration signal is extracted from the displacement field of each 2D image. This respiration signal is used to synchronize the 2D image series to the respiratory cycle at every table position. After the synchronization, the displacement field for the entire lung volume at every selected respiratory phase is reconstructed, interpolated, and smoothed. The 4D lung images are reconstructed by a deformable transformation of the reference volume for the entire respiratory cycle.

Registration of 2D Image to Reference CT Volume

The deformable registration between a 2D slice and the reference volume includes three key steps: lung segmentation, local image registration, and propagation of local image registration. Although the lung segmentation is the first step of the 2D/3D registration, the segmentation will be described in the end of this section for a clearer presentation of the algorithm.

Local image registration.—To calculate the deformation of the 2D image with respect to the reference volume, we divide the 2D image into small overlapping disk regions, and register each of the small regions piece by piece to the reference volume. This algorithm is inspired by the block matching algorithm (13) that is a standard technique for object tracking and motion analysis in video

sequences (14). The local registration algorithm is based on minimizing the zero mean sum of squared differences (ZMSSD) (15) between a small region in the 2D image and a corresponding region in the reference volume. The size of the analysis region is mainly an empirical choice, which affects the accuracy, robustness, and computation time of the algorithm. We set the radius of the analysis region to be 20 pixels in our implementation. Several models, including rigid-body, affine, quadratic, and cubic transformations, have been tested to model the deformation between the 2D region and the 3D region. It is observed that the quadratic transformation usually results in the smallest residual error under the selected region size. Equation 1 shows the formula of quadratic transformation.

$$T(x, y, z, \mu)$$

$$= \begin{pmatrix} a_{00} & a_{01} & a_{02} & a_{03} & a_{04} & a_{05} & a_{06} & a_{07} & a_{08} & a_{09} \\ a_{10} & a_{11} & a_{12} & a_{13} & a_{14} & a_{15} & a_{16} & a_{17} & a_{18} & a_{19} \\ a_{20} & a_{21} & a_{22} & a_{23} & a_{24} & a_{25} & a_{26} & a_{27} & a_{28} & a_{29} \\ 0 & 0 & 0 & 0 & 0 & 0 & 0 & 0 & 0 & 1 \end{pmatrix} \begin{pmatrix} x^2 \\ y^2 \\ z^2 \\ xy \\ yz \\ zx \\ x \\ y \\ z \\ 1 \end{pmatrix} \quad (1)$$

where (x,y,z) is a voxel's position in a 2D image region, $T(x,y,z,\mu)$ is the voxel's position in the reference volume, and $\mu = \{a_{00}, a_{01}, \dots, a_{29}\}$ is the parameter vector to be estimated.

The quadratic model allows the 2D region to be warped and shifted in 3D to match the lung anatomy of the reference volume. Thirty parameters need to be estimated for each local registration while the objective function is optimized. To increase the robustness of the local registrations, an affine transformation is applied before using the quadratic model to estimate some of the parameters $\{a_{06} \sim a_{09}, a_{16} \sim a_{19}, a_{26} \sim a_{29}\}$. The remaining parameters are set to zero to generate a starting point for the quadratic model-based optimization. Equation 2 shows the objective function of the local registration. The Gauss-Newton method is used to solve the optimization problem.

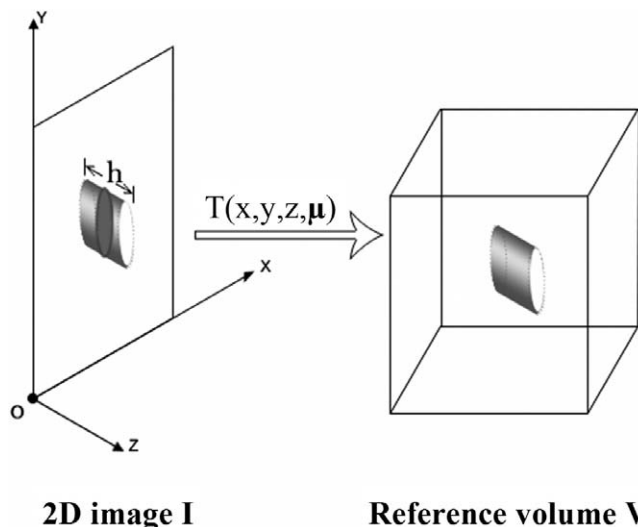


Figure 2. Local image registration.

$$O(\mu) = \sum_{(x,y) \in \Omega} \left\{ \left[\frac{1}{h} \int_{z=-h/2}^{z=h/2} v(T(x,y,z,\mu)) dz - \hat{V}_{mean} \right] - [I(x,y) - \hat{I}_{mean}] \right\}^2 \quad (2)$$

where I is the 2D image, V is the reference volume, and h is the slice thickness of the 2D image as shown in Fig 2. \hat{I}_{mean} and \hat{V}_{mean} are the average intensities of a 2D region and its correspondence in 3D. More details about the local registration using an affine model have been described previously (16).

Propagation of local image registration.—Because the ZMSSD registrations are performed locally, there is no guarantee that all the registrations converge correctly. A global regularization of the local registrations is necessary to remove outliers. In an example shown in Fig 3, the regions are partially overlapped on each other. Because pixel p is included in all the disk regions $A_0, A_1,$ and A_2 , the deformation of pixel p can be calculated from every one of these regions. As shown in Eq 3, the final deformation of pixel p is the weighted average of all deformations obtained from the overlapped regions.

$$\hat{d}(x, y) = \sum_k r_k c_k g_k w_k(x, y) d_k(x, y) \quad (3)$$

where d_k is the pixel displacement obtained from the k^{th} region; \hat{d} is the weighted average of the displacement; and r_k is a function of the residual error of the ZMSSD

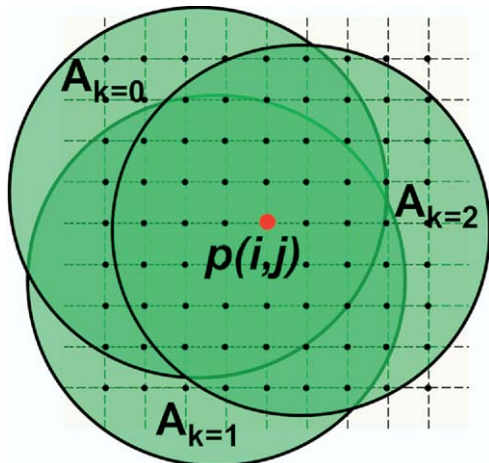
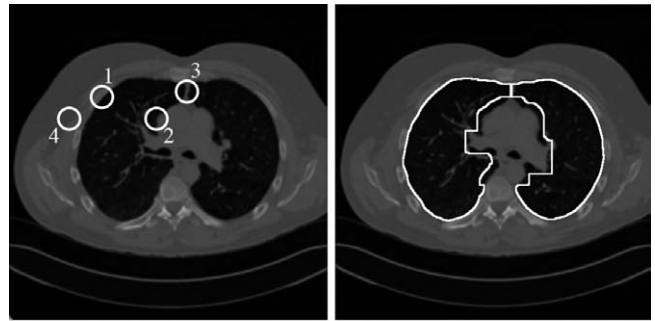


Figure 3. Propagation of local registration.

similarity measure of the k^{th} region. r_k will be assigned a large value for small residual error, and vice versa. r_k will be zero if the residual error of a region is above a threshold. c_k is a function of the registration consistency in the overlapping area between the current region k and the regions that have already been registered. c_k will be large if the consistency is high; otherwise, c_k will be small. c_k will be zero if the difference between the current registration results and the previous registration results is too large. The assumption is that the results from previous registrations are more likely to be correct, because they are the weighted averages of many local registrations. w_k is a Gaussian window function that is centered on the region k , giving the registration results of central pixels a larger weight. This is because the deformable model fits better in the highly clustered central area than the less clustered peripheral areas. For the same reason, we use a circular region instead of a classical rectangular region for local registrations. As a result, Eq. (3) filters out failed and bad registrations and assigns large weight to good registrations. Unlike other registration techniques going from coarse to fine resolution, this registration goes from local to global. The algorithm iteratively propagates its local registrations, allowing the deformation of regions without enough texture information to be correctly estimated. Equation 3 also globally regularizes the local registrations, smoothing the displacement field of the 2D slice.

In this propagation method, pixels computed earlier have larger effects on the algorithm than pixels computed later because the results of earlier local registrations are used to initialize and evaluate later registrations. To improve the robustness of early registrations, every step of the propagation is performed on the boundary of the



a.

b.

Figure 4. (a) Undesired regions: 1) both lung pixels and chest-wall pixels are included; 2) both lung pixels and heart pixels are included; 3) both left and right lungs are included; and 4) other non-lung pixels are included. (b) The result of lung segmentation. Note that the blood vessels are preserved; the heart and chest-wall are removed; the left and right lungs are separated; and the marginal pixels are removed from the heart-lung boundary.

propagated area where the analysis region has the strongest texture information.

Lung segmentation.—The region-based algorithm assumes the pixels of the region to have approximately the same type of motion. It is necessary that all the pixels in the region are lung pixels. If the region includes other pixels such as heart pixels (Fig 4a, circled region 2), the registration is prone to fail, because the selected deformation models cannot explain the pixel motion of the analysis window. For the same reason, the region cannot have chest wall pixels (Fig 4a, circled region 1), nor can the region have pixels from both the left and right lungs (Fig 4a, circled region 3). Therefore, accurate lung segmentation is necessary before the registration, and the left and right lungs should be separated in the 2D images.

We adopted the techniques of Hu (17) to automatically segment the lungs in the 2D image. Based on their work, additional morphologic image processing is executed on the lung area to keep the small to middle blood vessels in the lungs. Extra margin is also introduced in the heart-lung boundary to exclude the artifact caused by the cardiac motion. The result of lung segmentation is shown in Fig 4b. It should be noted that this segmentation algorithm does not separate different lung lobes. Therefore, it is possible for an analysis region to include pixels from different lobes. If discontinuous motion is large between lung lobes, the local registrations near the lobe interface may fail or generate large registration error. In that case, the algorithm will suppress the effect of these local registrations with a small r_k in Eq. (3), and rely on the registration results of the neighboring regions.

4D Lung Reconstruction

After all the 2D slices are registered to the reference volume, the average displacement of lung pixels of each slice is calculated, yielding a 3D vector that represents the gross motion of the slice with respect to the reference volume. For a 2D image series taken at the same table position while the patient is breathing freely, a sequence of gross motion vectors can be obtained. This vector sequence has phase information of respiratory motion and therefore can be used to synchronize the 2D image series with the respiratory cycle. As an example, if a 2D image has the smallest gross motion among a 2D image series obtained at the same table position, this image can be considered to have (approximately) the same respiratory phase as the reference volume and vice versa.

The synchronization procedure is performed as follows. First, we correlate two gross motion sequences at every two adjacent table positions. Because lung deformation is continuous, this correlation is conducted between two similar gross motion vectors with a time shift. Therefore, the correlation is reliable. The correlation can be calculated using the following formula:

$$S = \arg \max_j \sum_{k=0}^{N-1} (\Delta x_k \Delta x'_{j+k} + \Delta y_k \Delta y'_{j+k} + \Delta z_k \Delta z'_{j+k}) \quad (4)$$

where N is the total number of frames to be correlated; $(\Delta x_k, \Delta y_k, \Delta z_k)$ is gross motion of the k^{th} image frame in one 2D series; $(\Delta x'_k, \Delta y'_k, \Delta z'_k)$ is gross motion of the k^{th} image frame in another 2D series obtained at an adjacent table position; and S is the number of frame shifts between the two image sequences. Temporal interpolation can be used if the frame rate of the 2D scan is low. By repeating this correlation at all table positions, all the 2D series can be synchronized. The assumption is that lung areas at different table positions reach their peak motion at the same time. In other words, there is no phase variation of respiratory motion along the craniocaudal direction. This assumption will be addressed later in the experiment section of this article. After all 2D series are synchronized, the average length of the respiratory cycle is estimated. For 2D series obtained in irregular respiratory cycles, the length of the 2D series may need to be cut or extended near the end-expiration to meet the average length of the respiratory cycle. Because respiratory motion changes very little near the end-expiration, the impact of this approximation on the result is small.

The motion vector of each 2D image is three-dimensional. It is desirable to reduce it to one dimension to

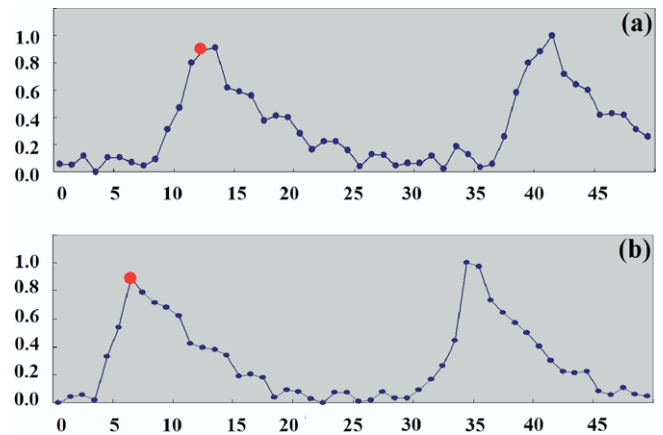


Figure 5. Normalized respiration signals at two adjacent table positions extracted from swine study.

represent the respiratory phase. Therefore, the principal axis of the motion trajectory is calculated using principal component analysis. The one-dimensional respiration signal can be extracted by projecting the average motion on the principal axis. Figures 5a and 5b show the normalized respiration signals of two CT fluoroscopy image series obtained in a swine study at two adjacent table positions with an interval of 4 mm. It can be observed that the CT fluoroscopy scan time of the two sequences was different with respect to the respiratory cycle. The two dots on the peaks of the respiration signals show the result of synchronization.

After all the 2D image series are synchronized, the 4D lung can already be reconstructed by sorting the 2D images (9) according to their table positions and respiratory phases. However, because the 2D images come from different respiratory cycles where respiratory motion may not be completely reproducible, the 4D reconstruction by sorting 2D images can have very poor image quality. Especially in the coronal and sagittal views, fuzzy edges are usually observed.

To improve the image quality, we use a different approach to reconstruct the 4D dataset. First, we reconstruct the displacement fields of the lungs at every respiratory phase. This step only needs very little computation time because the displacement field of every 2D image has already been obtained from the deformable registration. The deformation of the entire lung volume is calculated by combining the 2D images' displacement fields according to their table positions and respiratory phases.

The resulting displacement field from the first step reflects deformation of the lungs at a respiratory phase. This displacement field may not be smooth along the

craniocaudal direction because it is obtained from multiple respiratory cycles that may not be exactly repeatable. Therefore, our second step is to smooth the displacement field in the craniocaudal direction (eg, using a Gaussian filter). It should be noted that this smoothing operation is not applied on image values; therefore, the reconstructed 4D data will not be degraded. The effect of the smoothing operation is similar to “averaging” irregular respiratory motion obtained from different respiratory cycles. Additionally, if the 2D scan covers more than one respiratory cycle at a table position, it is desirable to obtain an average displacement field for the table position to alleviate the degradation of irregular respiration on 4D CT. After the smoothing operation, the displacement field of the entire lung volume is obtained by interpolating the smoothed displacement fields of 2D slices in the craniocaudal direction (using B-spline [18] or linear interpolation).

Finally, we compute the 3D volume at any respiratory point by a deformable transformation of the reference volume. As a feature of the algorithm, the spatial resolution of the constructed 4D data is determined by the resolution of the reference volume.

RESULTS

Three experiments were conducted to validate the algorithm. These experiments were based on a synthetic 4D CT, a swine study, and a clinical 4D CT, respectively.

Experiments on Synthetic 4D CT

The goal of the first experiment is to validate the accuracy of the deformable registration between a 2D image slice and the reference CT volume. A synthetic 4D dataset was used in the experiment.

The synthetic 4D data was contributed by Siemens Corporate Research and generated from two lung volumes obtained at end-inspiration and end-expiration, respectively. The two volumes were registered using an independent deformable registration algorithm. The displacement field between the two volumes was interpolated along the time axis such that the trajectory of each pixel is a 3D curve in space instead of a straight line (19). As shown in Fig 6, the resulting 4D data were used as the ground truth to validate the 4D algorithm. The synthetic 2D free scan image series was obtained by sampling the 4D data at a selected table position. With the 2D image series and the lung volume at the end expiration as the reference volume, we ran the algorithm to

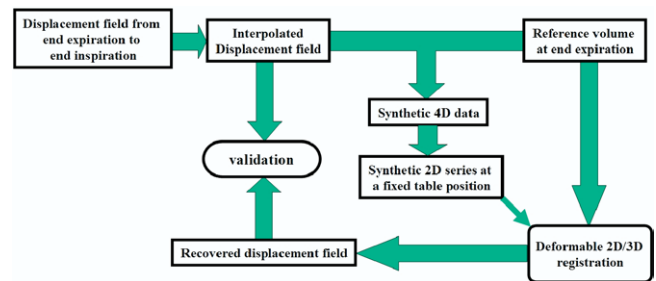


Figure 6. Validation of two-dimensional/three-dimensional deformable registration.

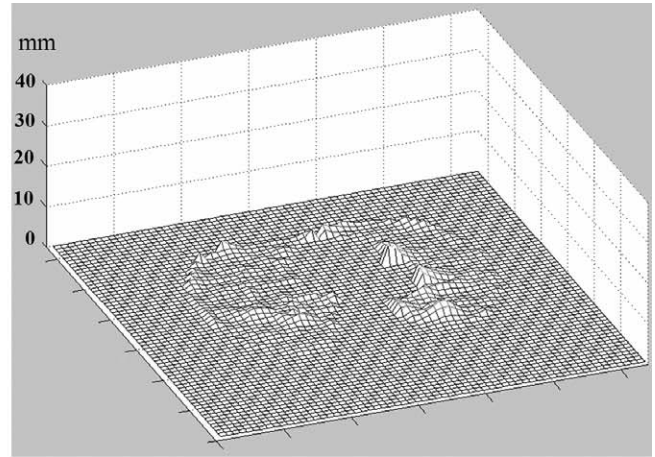
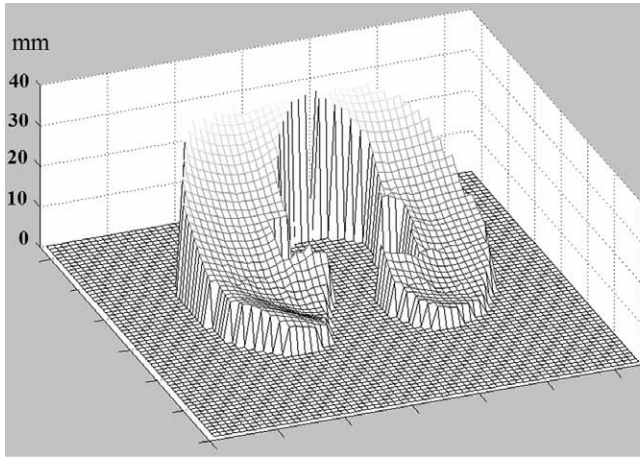
recover the lung deformation. The pixel size of both the preoperative CT volume and the 2D images was 0.74 mm. The slice thickness of the preoperative CT volume was 1.25 mm and 3.75 mm for the synthetic 2D free scan images. The results were first compared with the ground truth to validate the deformable 2D/3D registration.

Figure 7 shows the deformation magnitude of a 2D image taken at end-inspiration when the 2D image has the largest deformation with respect to the reference CT volume. As shown in Fig 7, most of the poor registrations happen on the boundary pixels of the lungs. This problem has three causes. First, for the region-based algorithm, the registration accuracy is usually higher for the pixels near the center of the analysis region; the boundary pixels of lung are usually far from the center of the analysis region. Second, the boundary pixels (especially the boundary pixels near the anterior lung) have larger deformation than the average. Third, the areas near the lung boundary often have little texture information, which may not be enough for the local image registration.

Figure 8 shows the average registration error and the standard deviation of the error as opposed to gross slice motion. The maximum average error is below 0.6 mm, or 5% of gross slice motion (for large respiratory motion). It can be observed that both the registration error and the standard deviation increase as the deformation of the 2D slice increases, suggesting that the deformable model has the better performance for smaller deformation of the lungs.

Experiments on Swine Study

The second experiment was a swine study as part of an approved animal protocol. This study was done at Georgetown University Medical Center on a Siemens Somatom Volume Zoom four-slice CT/CT fluoroscopy scanner. The reference volume was obtained at end-expi-



a. **Figure 7.** (a) Displacement magnitude of a two-dimensional image with respect to the reference computed tomography volume in millimeters. (b) Magnitude of registration error in millimeters.

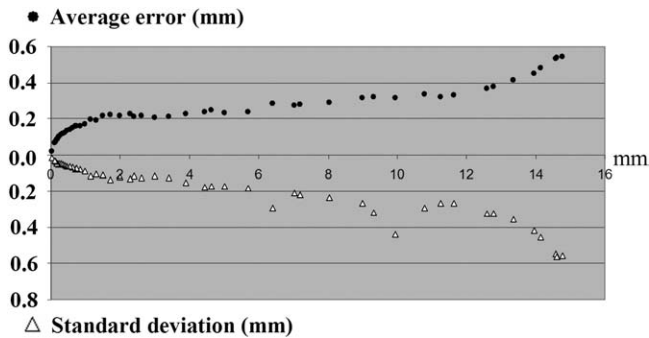
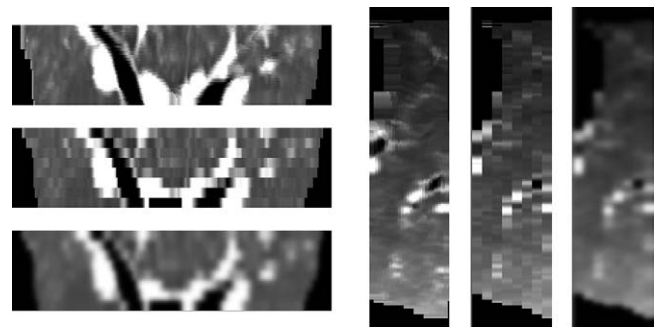


Figure 8. Registration error and standard deviation vs. magnitude of gross slice motion.

ration using a 1-mm slice thickness. The animal was mechanically ventilated, and during the image acquisition the ventilator was turned off and the animal was temporarily paralyzed to minimize any breathing artifacts. The 2D image series were acquired using CT fluoroscopy with a sample rate of 6 Hz and a slice thickness of 4 mm. Ten 2D image series were acquired. **Figures 9a** and **9b** show the reconstruction results at end of inspiration, which is the respiratory phase of the maximum deformation with respect to the reference volume. As shown in the figures, the reconstruction result of our algorithm is much smoother compared with the image-sorting method and less blurred compared with the image-sorting method with Gaussian smoothing.

Experiments on Respiratory Gated 4D CT

The main purpose of the third experiment was to test the consistency between our algorithm and other 4D CT



a. **Figure 9.** Coronal and sagittal views of four-dimensional reconstruction in a swine study. The top image of (a) and the left image of (b) are results of our method. The middle images of (a) and (b) are results of the image sorting method. The bottom image of (a) and the right image of (b) are results of the image sorting method with Gaussian smoothing.

algorithms. A clinical 4D CT dataset was used as the ground truth, which included 10 CT volumes obtained at 10 respiratory phases using respiratory gating. The CT volume at end-expiration was selected as the reference volume with a slice thickness of 2 mm. The 4D dataset was then resliced with 6-mm slice thickness at a series of table positions to simulate 2D image time sequences. Each 2D image was registered to the reference volume to obtain the displacement field as an example shown in **Fig 10**.

Because the real 4D CT dataset was acquired in 10 different respiratory phases, the reslicing operation at each table position yielded a 2D series of 10 images associated with these respiratory phases. **Figure 11b** shows the

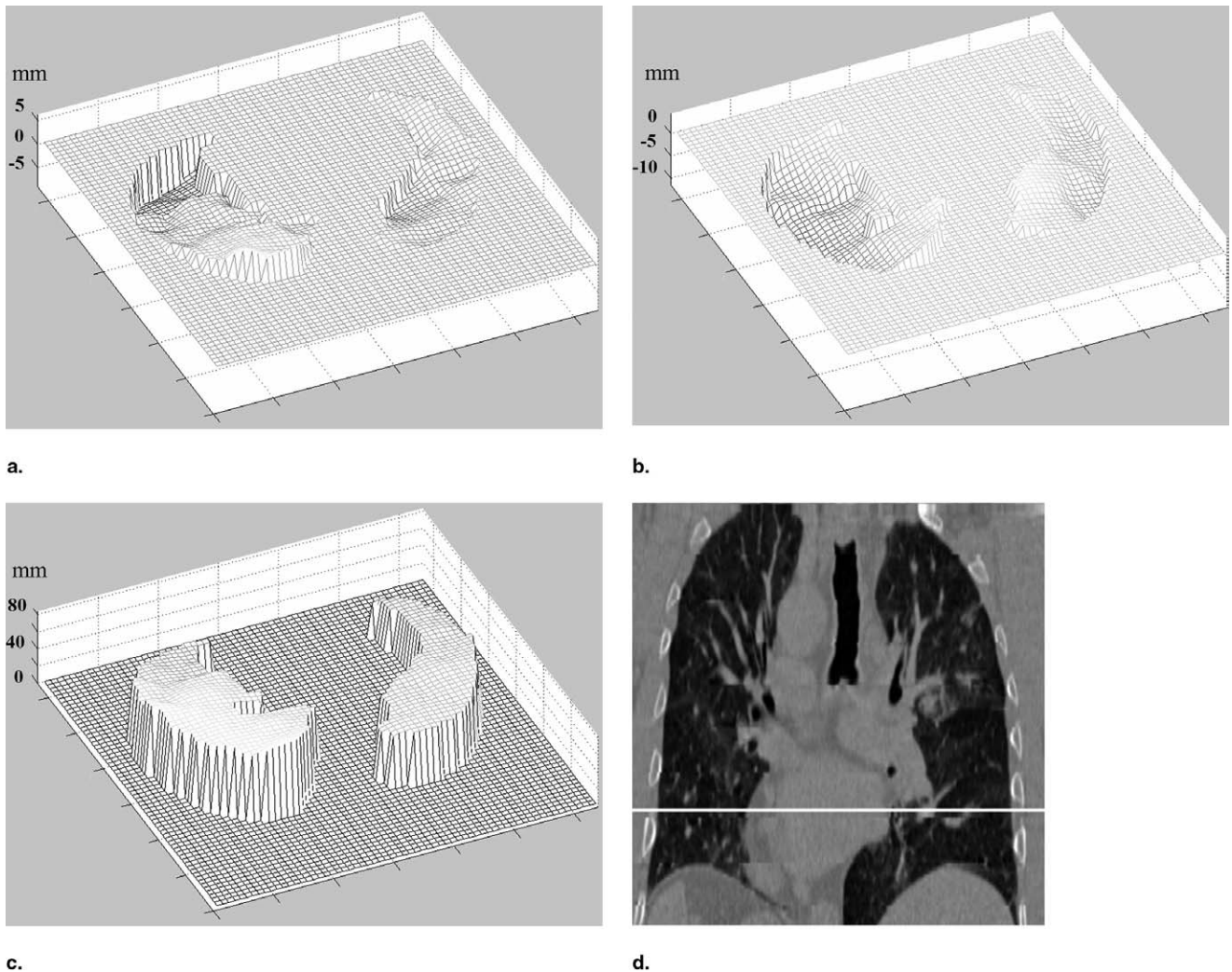


Figure 10. Displacement field of a two-dimensional slice. Note that the scales are different for each component. **(a)** X component. **(b)** Y component. **(c)** Z component. **(d)** Slice position in coronal view.

average displacements of two 2D image series obtained at the upper lung and the lower lung as labeled in Fig 11a. Our algorithm was used to recover the 4D data between the two slices. It can be seen that the respiratory phase at the lower lung lagged behind the upper lung (Fig 11b). The deformation of other lung slices also confirm that phase variation of respiratory motion exists along the craniocaudal direction, meaning that the average motion of each 2D image may not be accurate to synchronize 2D image sequences at different table positions. To estimate the impact of the phase variation, the 4D reconstruction result of our algorithm was compared with the original respiratory-gated 4D data. Figure 11c shows a coronal image of the 4D data reconstructed at end inspiration as-

suming that all lung slices reach their maximum deformation at the same time.

The respiratory-gated 4D data shown in Fig 11a was used as the ground truth to validate our algorithm. The difference between the ground truth and the reconstructed data is shown in Fig 11e, which consists of both the registration error and the phase variation error. It can be observed from the difference image that many of the major airways and blood vessels were removed, meaning that the 4D reconstruction remains reasonably accurate under phase variation of respiratory motion.

Another goal of the third experiment was to evaluate the effect of the spatial scan interval to our algorithm. Because the algorithm interpolates the displacement field

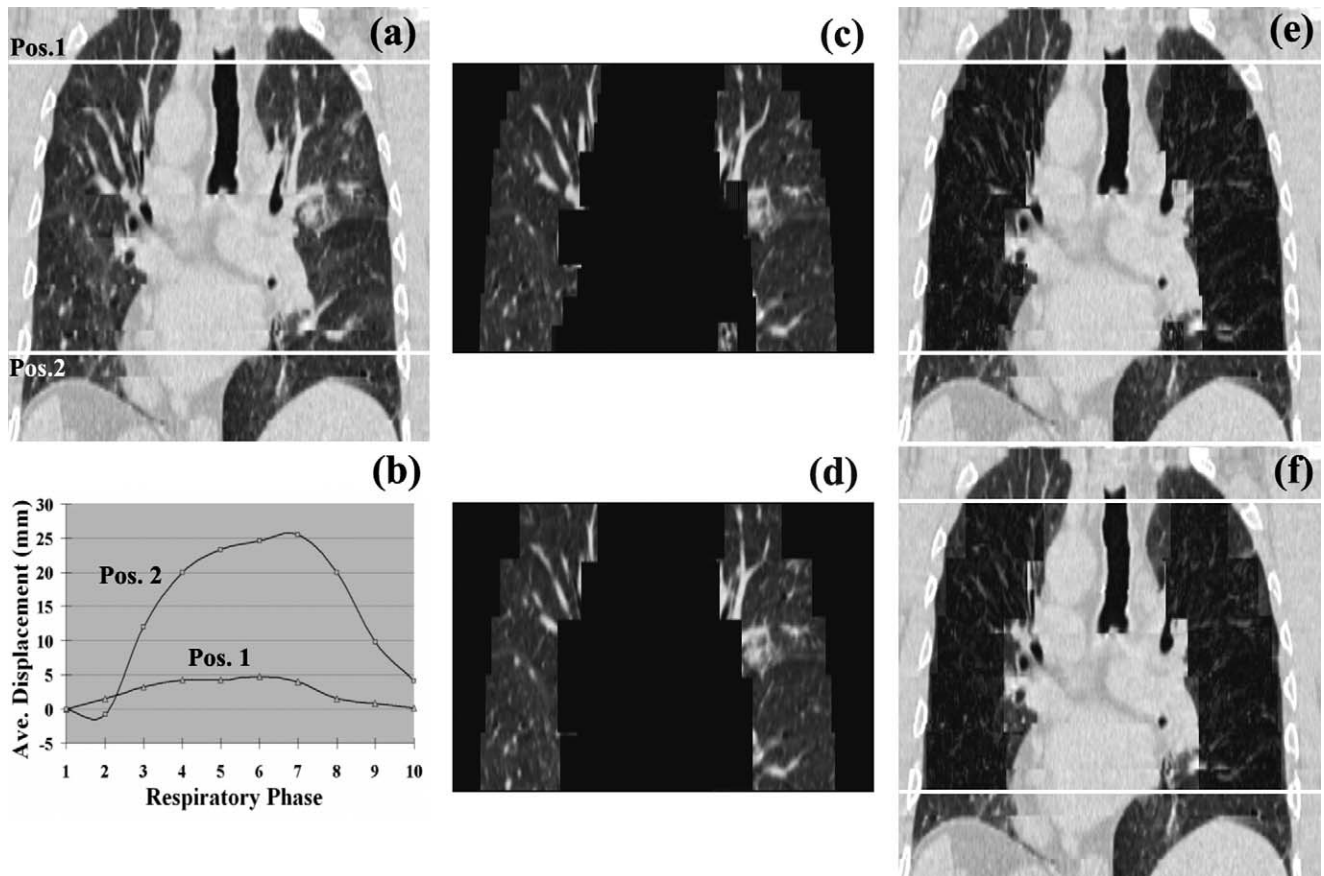


Figure 11. (a) A coronal slice of the ground truth four-dimensional data at end-inspiration. (b) Respiration signals of a slice at the upper lung and a slice at the lower lung labeled in (a). (c) A coronal slice of the reconstructed four-dimensional data with 10-mm scan interval. (d) A coronal slice of the reconstructed four-dimensional data with 20-mm scan interval. (e) The difference of (a) and (c). (f) The difference of (a) and (d).

between consecutive table positions, larger scan interval can reduce the number of 2D image scans and thus lower the radiation dose to the patient. At the same time, sparser scans along the CT table may also degrade the accuracy of the reconstructed 4D data. To validate the impact, we compared the reconstruction results obtained with two different scan intervals: 10 mm (Fig 11c) and 20 mm (Fig 11d). These two reconstructed images were then subtracted from the ground truth image (Fig 11a). The reconstructed 10-mm scan (Fig 11e) shows smoother lung boundaries than the result of 20-mm scan (Fig 11f).

The numerical results of Fig 11 are shown in Table 1. Because the 2D images are resliced from the real 4D data, their true synchronization is known. Although our algorithm cannot obtain this perfect synchronization in reality, the residual errors of the perfect synchronization were used in our experiment as a baseline for comparison. The last row of the table shows the absolute differ-

ence between the reference volume and the end-inspiration volume without registration.

Table 1 shows that the results of our synchronization (the approximated synchronization) and the perfect synchronization are close. There is no significant difference between the residual errors of the 10-mm scan and the 20-mm scan, suggesting that 4D CT data may be able to be reconstructed with reasonable accuracy by sparsely sampling CT table positions to reduce the radiation dose to the patient during image acquisition.

DISCUSSION

This article presents a new methodology to reconstruct a 4D lung image from a set of 2D CT scans and a reference CT volume. The temporal resolution of the method is high and the reconstruction provides good-quality images. Based on a synthetic CT data set, the average regis-

Table 1
Residual Errors Between the Reference Volume and the Reconstructed Volume in Hounsfield units (HU) per Voxel Under Two Scan Intervals

Scan Interval	10 mm	20 mm
Average residual error under perfect synchronization	71.26 HU/voxel	74.41 HU/voxel
Average residual error under approximated synchronization	80.74 HU/voxel	81.07 HU/voxel
Initial volume difference (without deformable registration)	148.55 HU/voxel	

tration error was less than 5% of the average lung deformation. Results from a swine study also showed that better image quality can be obtained using the algorithm instead of the image sorting method.

The algorithm is software-based. It does not need any auxiliary surrogates to synchronize image scans with the respiratory phase. The image reconstruction quality of the algorithm is high even under irregular respiratory motion. The lesion's trajectory can be obtained automatically. The algorithm may also allow for a reduction in the radiation dose to the patient by sparsely scanning CT table positions with a very limited loss of image quality.

One drawback of the algorithm is that it is time consuming. It takes several minutes to register a 2D image slice to the reference volume, depending on the size of the lung area in the image. However, it should be noted that the algorithm can reconstruct a 4D subvolume by performing local registrations around the tumor, which can greatly reduce the computing time. The algorithm's architecture also allows it to be implemented on a parallel processing machine, if further improved processing speed is needed. Another limitation of the algorithm is that it cannot analyze respiratory motion in the most superior and inferior of the lungs. Because the deformable registration relies on texture information of the lungs, if soft tissue (eg, the diaphragm) does not have much texture under CT, the algorithm cannot register it when it moves in and out of the 2D axial slice.

Although the algorithm can be affected by phase variation of respiratory motion, the algorithm still showed reasonable accuracy in comparison to a respiratory-gated 4D dataset. Because respiratory motion of tumors is no more than a few centimeters in the craniocaudal direction, the phase variation can usually be ignored in treatment planning. However, the phase variation may become an important issue if 4D CT is used to assist real-time motion compensation, because small temporal errors may introduce large spatial errors depending on the speed of respiratory motion.

The algorithm was only tested on single-slice 2D scans in our experiments. The algorithm can be easily extended for use with multislice CT. Because multislice CT provides more texture information to the local region registration, this may result in higher accuracy and better robustness of the algorithm. Additionally, if two multislice image scans at two adjacent table positions are partially overlapped, the phase variation error can be accounted for by registering (or synchronizing) the overlapped slices.

One question raised by this research is the optimal number of respiratory phases (or temporal samples) for the 4D CT dataset. Intuitively, the number of respiratory phases should be a tradeoff between the resolution of the 4D dataset and the radiation dose to the patient. In terms of the resolution, the number of temporal samples can be determined by the maximum speed of respiratory motion. Therefore, the inspiration phase may need more samples than the expiration phase, and the lower lung may need more temporal samples than the upper lung. The number of temporal samples also depends on prior knowledge of respiratory motion. If the trajectory of each lung voxel can be modeled (eg, as a straight line), very few temporal samples will be needed.

ACKNOWLEDGMENT

The authors gratefully thank Frank Sauer, PhD, Ali Khamene, PhD, and Christophe Chef d'hotel, PhD, at Siemens Corporate Research for providing the lung dataset. The dataset was originally obtained by the EMC in Rotterdam. The authors also thank David Lindisch, RT, for his assistance with the experiments at Georgetown University.

REFERENCES

1. US Cancer Statistics Working Group. United States cancer statistics: 1999–2002 incidence and mortality web-based report version. Atlanta (GA): Department of Health and Human Services, Centers for Disease Control and Prevention, and National Cancer Institute; 2005.

2. Keall P. 4-dimensional computed tomography imaging and treatment planning. *Semin Radiat Oncol* 2004; 14:81–90.
3. El Naqa IM, Low DA, Christensen GE, et al. Automated 4D lung computed tomography reconstruction during free breathing for conformal radiation therapy. In: Amini AA, Manduca A, eds. *Medical imaging 2004: Physiology, Function, And Structure From Medical Images*; San Diego, Ca: 2004; 100–106.
4. Ohara K, Okumura T, Akisada M, et al. Irradiation synchronized with respiration gate. *Int J Radiat Oncol Biol Phys* 1989; 17:853–857.
5. Kubo HD, Wang L. Introduction of audio gating to further reduce organ motion in breathing synchronized radiotherapy. *Med Phys* 2002; 29: 345–350.
6. Shirato H, Shimizu S, Kunieda T, et al. Physical aspects of a real-time tumor-tracking system for gated radiotherapy. *Int J Radiat Oncol Biol Phys* 2000; 48:1187–1195.
7. Boldea V, Sarrut D, Clippe S. Lung deformation estimation with non-rigid registration for radiotherapy treatment. In: Ellis RE, Peters TM, eds. *Medical image computing and computer-assisted intervention. Lecture Notes in Computer Science* 2003; Springer-Verlag Berlin Heidelberg; 770–777.
8. Vedam SS, Keall PJ, Kini VR, et al. Acquiring a four-dimensional computed tomography dataset using an external respiratory signal. *Phys Med Biol* 2003; 48:45–62.
9. Underberg RW, Lagerwaard FJ, Cuijpers JP, et al. Four-dimensional CT scans for treatment planning in stereotactic radiotherapy for stage I lung cancer. *Int J Radiat Oncol Biol Phys* 2004; 60:1283–1290.
10. Wong JW, Sharpe MB, Jaffray DA, et al. The use of active breathing control (ABC) to reduce margin for breathing motion. *Int J Radiat Oncol Biol Phys* 1999; 44:911–919.
11. Pan T, Lee TY, Rietzel E, et al. 4D-CT imaging of a volume influenced by respiratory motion on multi-slice CT. *Med Phys* 2004; 31: 333–340.
12. Ford EC, Mageras GS, Yorke E, et al. Respiration-correlated spiral CT: a method of measuring respiratory-induced anatomic motion for radiation treatment planning. *Med Phys* 2003; 30:88–97.
13. Watkinson J. *MPEG handbook*. Focal Press, UK, 2001.
14. Hager G, Belhumeur P. Efficient region tracking with parametric models of geometry and illumination. *IEEE Trans Pattern Anal Machine Intelligence* 1999; 20:1205–1039.
15. Rehg JM, Witkin AP. Visual tracking with deformation models. *Proc IEEE Int Conf Robotics Automation* 1991;(1)844–850.
16. Xu S, Fichtinger G, Taylor RH, et al. 3D motion tracking of pulmonary lesions using CT fluoroscopy images for robotically assisted lung biopsy. In: Galloway RL Jr, eds. *Medical imaging 2004: visualization, image-guided procedures, and display*. San Diego, Ca: 2004; 394–402.
17. Hu S, Hoffman EA, Reinhardt JM. Automatic lung segmentation for accurate quantitation of volumetric X-ray CT images. *IEEE Trans Med Imaging* 2001; 20:490–498.
18. Unser M. Splines—a perfect fit for signal and image processing. *IEEE Signal Proc Mag* 1999; 16:22–38.
19. Xu S, Fichtinger G, Taylor RH, et al. Validation of 3D motion tracking of pulmonary lesions using CT fluoroscopy images for robotically assisted lung biopsy. In: Galloway RL Jr, Cleary KR, eds. *Medical imaging 2005: Visualization, image-guided procedures, and display*. San Diego, Ca: 2005; 60–68.